



HAL
open science

Allosterically Regulated Guest Binding Determines Framework Symmetry for an Fe II 4 L 4 Cage

Weichao Xue, Kai Wu, Nianfeng Ouyang, Thierry Brotin, Jonathan R Nitschke

► **To cite this version:**

Weichao Xue, Kai Wu, Nianfeng Ouyang, Thierry Brotin, Jonathan R Nitschke. Allosterically Regulated Guest Binding Determines Framework Symmetry for an Fe II 4 L 4 Cage. *Angewandte Chemie International Edition*, 2023, 62 (18), pp.e202301319. 10.1002/anie.202301319 . hal-04218728

HAL Id: hal-04218728

<https://hal.science/hal-04218728v1>

Submitted on 26 Sep 2023

HAL is a multi-disciplinary open access archive for the deposit and dissemination of scientific research documents, whether they are published or not. The documents may come from teaching and research institutions in France or abroad, or from public or private research centers.

L'archive ouverte pluridisciplinaire **HAL**, est destinée au dépôt et à la diffusion de documents scientifiques de niveau recherche, publiés ou non, émanant des établissements d'enseignement et de recherche français ou étrangers, des laboratoires publics ou privés.

Metal-Organic Cages

Allosterically Regulated Guest Binding Determines Framework Symmetry for an Fe^{II}₄L₄ Cage

Weichao Xue, Kai Wu, Nianfeng Ouyang, Thierry Brotin, and Jonathan R. Nitschke*

Abstract: Self-assembly of a flexible tritopic aniline and 3-substituted 2-formylpyridine subcomponents around iron(II) templates gave rise to a low-spin Fe^{II}₄L₄ capsule, whereas a high-spin Fe^{II}₃L₂ sandwich species formed when a sterically hindered 6-methyl-2-formylpyridine was used. The Fe^{II}₄L₄ cage adopted a new structure type with S₄ symmetry, having two *mer-Δ* and two *mer-Λ* metal vertices, as confirmed by NMR and X-ray crystallographic analysis. The flexibility of the face-capping ligand endows the resulting Fe^{II}₄L₄ framework with conformational plasticity, enabling it to adapt structurally from S₄ to *T* or C₃ symmetry upon guest binding. The cage also displayed negative allosteric cooperativity in simultaneously binding different guests within its cavity and at the apertures between its faces.

Biological receptors can dynamically adapt to optimize binding affinity, thus enhancing or inhibiting signal transduction in living systems.^[1] Allosteric regulation, whereby biological receptors transmit the effect of binding a substrate at one site to another at a distant site, is an essential process by which natural systems process information.^[2] The development of artificial allosteric systems, which are capable of emulating the biologically occurring processes of activity regulation, can enable new applications,^[3] but these systems are challenging to design.^[4]

Metal-organic cages formed by coordination-driven self-assembly, with well-defined cavities and binding sites, have emerged as a powerful platform for the modular design of biomimetic supramolecular systems. These cages have also proven useful across diverse areas, including molecular recognition and sensing,^[5] chemical separation,^[6] stabilization of otherwise unstable species,^[7] and catalytic transformations.^[8] The reversible linkages between metal

vertices and coordination sites can enable these cages to disassemble and reassemble in response to external stimuli,^[9] for instance, temperature,^[10] light,^[11] redox,^[12] and pH.^[13]

Most cages contain symmetric and rigid ligands, which produce high-symmetry structures resembling Platonic and Archimedean solids, such as tetrahedra,^[14] octahedra,^[15] cubes,^[16] cuboctahedra^[17] and other higher-order structures.^[18] The high symmetry of such synthetic hosts differentiates them from biological systems, as natural receptors are rarely isotropic, highly symmetric species.^[19] To this end, the rational design of low-symmetry host systems with inherent conformational adaptability is needed, in order to study intricate binding behaviors in adaptable chemical systems, which may lead to the development of bioinspired applications.

Here we present the synthesis of a S₄-symmetric Fe^{II}₄L₄ cage **1** by subcomponent self-assembly (Figure 1). This cage dynamically adapted upon guest encapsulation to form host-guest complexes with either lower (C₃) or higher (*T*) symmetry. The cage also simultaneously bound different guests at two distinct sites, with negative allosteric modulation observed between them.

Tritopic aniline subcomponent **A**, with a 1,3,5-tris(2-furyl)-2,4,6-trimethoxybenzene central core, was synthesized from commercially available 1,3,5-trimethoxybenzene over four steps (Figure S1). Steric clash between the furan rings and methoxy groups engenders a non-planar conformation of the central core. The three-dimensionality and structural flexibility of the core of **A** were elegantly exploited by Fujita, Takezawa et al. in a knotted cage prepared from a related ligand.^[20]

The reaction of trianiline **A** (4 equiv) and 3-nitro-2-formylpyridine **B** (12 equiv) with iron(II) bis(trifluoromethanesulfonyl)imide (Fe^{II}(NTf₂)₂, 4 equiv) in CD₃CN at 343 K for 2 h produced cage **1** (Figure 1a), with its Fe^{II}₄L₄ composition confirmed by electrospray ionization mass spectrometry (ESI-MS, Figure S11). The ¹H NMR spectrum of **1** exhibited three sets of magnetically-distinct proton signals, with all signals displaying the same diffusion coefficient in the ¹H diffusion-ordered spectroscopy (DOSY) spectrum (Figures 1b and S6). ¹H-¹H nuclear Overhauser effect (NOE) correlations between protons of pyridyl and phenylene rings were consistent with low-symmetry *meridional* (*mer*) configurations at the iron(II) centers (Figure S8).^[21] We therefore inferred Fe^{II}₄L₄ cage **1** to possess S₄ symmetry,^[22] in which all iron(II) centers adopt a *mer* stereochemical configuration, with two exhibiting *Δ* handedness, and the other two *Λ*.

[*] Dr. W. Xue, Dr. K. Wu, N. Ouyang, Prof. Dr. J. R. Nitschke
Yusuf Hamied Department of Chemistry, University of Cambridge
Cambridge CB2 1EW (UK)
E-mail: jrn34@cam.ac.uk

Dr. T. Brotin
Laboratoire de chimie, Université Lyon, Ens de Lyon, CNRS UMR
5182
69342 Lyon (France)

© 2023 The Authors. Angewandte Chemie International Edition published by Wiley-VCH GmbH. This is an open access article under the terms of the Creative Commons Attribution License, which permits use, distribution and reproduction in any medium, provided the original work is properly cited.

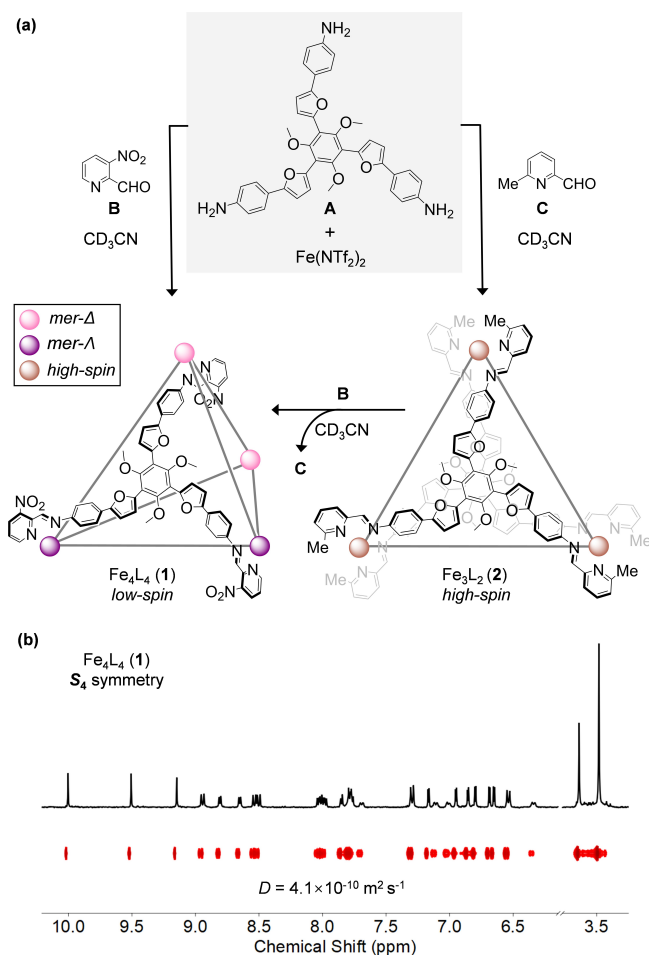


Figure 1. a) Subcomponent self-assembly of $\text{Fe}^{\text{II}}_4\text{L}_4$ capsule **1** and $\text{Fe}^{\text{II}}_3\text{L}_2$ sandwich **2** from **A**, $\text{Fe}^{\text{II}}(\text{NTf}_2)_2$ and 2-formylpyridines **B** and **C**, respectively. All reactions were performed at 343 K in CD_3CN . b) Partial ^1H NMR and DOSY spectra of S_4 -symmetric **1** (400 MHz, CD_3CN , 298 K), showing three sets of magnetically-distinct peaks.

In place of subcomponent **B**, other 2-formylpyridine derivatives were also attempted. Changing the substituent at the 3-position of the 2-formylpyridine did not affect the stereochemical outcome during self-assembly, with the formation of a series of $\text{Fe}^{\text{II}}_4\text{L}_4$ cages (**3–5**) possessing S_4 symmetry (Figures S14–S23).

Intriguingly, high-spin complex **2** was formed by the reaction of 6-methyl-2-formylpyridine **C** with **A** and $\text{Fe}^{\text{II}}(\text{NTf}_2)_2$ (Figure 1a), as confirmed by the wide-sweep ^1H NMR spectrum, with signals in the range -42 to 208 ppm (Figure S12). The ESI-MS spectrum confirmed the $\text{Fe}^{\text{II}}_3\text{L}_2$ composition of **2** (Figure S13). In accordance with the 18-electron rule,^[23] we inferred that each iron(II) vertex of **2** might be surrounded by two bidentate chelating units and two extra solvent molecules, with the high-spin character of **2** being a consequence of steric clash between methyl groups and the adjacent pyridyl rings around the iron(II) centers, as observed previously.^[24] By elongating the $\text{Fe}^{\text{II}}\text{--N}$ bonds, such steric repulsion also results in the destabilization of $\text{Fe}^{\text{II}}_3\text{L}_2$ **2** relative to $\text{Fe}^{\text{II}}_4\text{L}_4$ **1** species. The formation of shorter, stronger $\text{Fe}^{\text{II}}\text{--N}$ bonds in **1** was thus inferred to

drive subcomponent exchange during the conversion of **2** to **1**, following the addition of 2-formylpyridine **B** (Figures 1a and S24).

Although many attempts to grow single crystals of **1** were unsuccessful, X-ray quality crystals of $\text{Fe}^{\text{II}}_4\text{L}_4$ analog **3**, constructed from 3-bromo-2-formylpyridine, were obtained by slow vapor diffusion of diethyl ether into an acetonitrile solution of **3** (Figure 2a). The solid-state structure of **3** adopts idealized S_4 symmetry, consistent with the solution-state NMR data (Figures 2b and S15).

The structure of **3** consists of four face-capping ligands, with two ligands adopting a clockwise orientation and the other two anticlockwise. These ligands bridge four iron(II) vertices, two *mer- Δ* and two *mer- Λ* . The mean $\text{Fe}^{\text{II}}\text{...Fe}^{\text{II}}$ distance along the four edges between Δ and Λ metal centers is 18.1 ± 0.3 Å; the $\text{Fe}^{\text{II}}\text{...Fe}^{\text{II}}$ distance between the two *mer- Λ* metal centers (15.4 Å) is slightly longer than between the two *mer- Δ* metal centers (14.4 Å). A cavity volume of 986 Å³ for **3** was calculated using the MoloVol program.^[25]

In the structure of **3**, the three dihedral angles between the central phenyl ring and the furan rings within the same clockwise face-capping ligand were observed to differ (40.1° ,

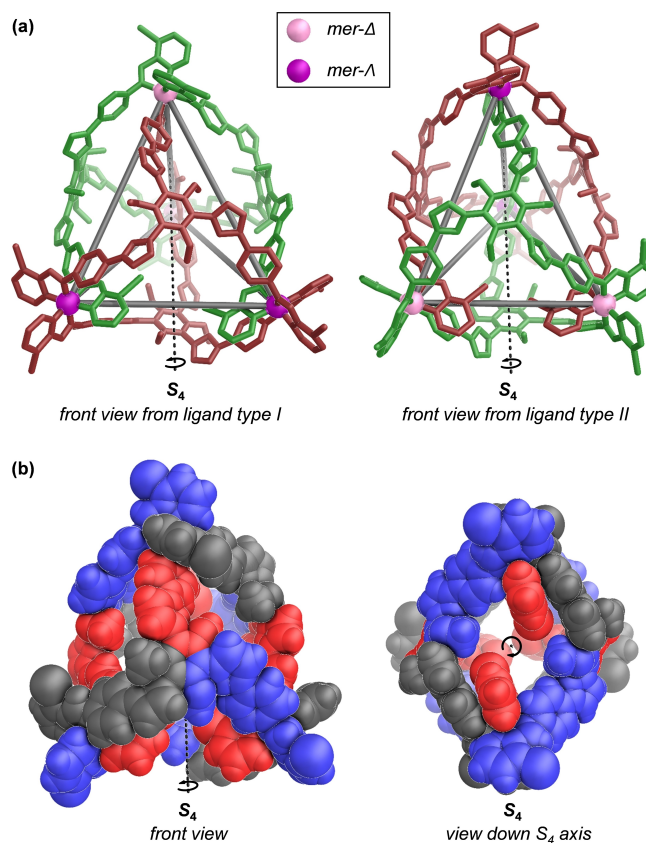


Figure 2. Different views of the crystal structure of $\text{Fe}^{\text{II}}_4\text{L}_4$ cage **3**, assembled from 3-bromo-2-formylpyridine, **A** and $\text{Fe}^{\text{II}}(\text{NTf}_2)_2$. a) Front views from ligand walls, with clockwise (type I) and anticlockwise (type II) oriented ligands colored brown and green, respectively. b) Front view and view down the *pseudo- S_4* axis, with the ligands shown in space-filling mode and the three magnetically-distinct environments shown in blue, red, and black. Disorder, anions, solvents and hydrogen atoms are omitted for clarity.

42.8°, 44.5°), as were the three torsion angles (52.2°, 58.2°, 62.2°) between the phenylene rings and the N–Fe^{II}–N chelate planes around each *mer-Λ* metal vertex. These differing angles thus reflect the structural flexibility and plasticity of the Fe^{II}₄L₄ framework to adopt different ligand configurations as required to minimize the energy of the system.

Table 1: Host-Guest Properties of **1**.

Guest ^[a]	K_a [M ⁻¹] ^[b]	Host Symmetry ^[c]
G1	$(1.82 \pm 0.05) \times 10^2$	S_4
G2	$(1.21 \pm 0.05) \times 10^2$	S_4
G3 ^[d]	$(2.33 \pm 0.10) \times 10^3$	T
G4	$(1.17 \pm 0.15) \times 10^5$	C_3

[a] ¹H NMR titrations were performed by the addition of aliquots of a CD₃CN solution of **G1** or **G2** (50 mM) into a stock solution of **1** in CD₃CN (0.5 mM); ¹H NMR titrations were performed by portionwise addition of **G3** or **G4** as a solid into a stock solution of **1** in CD₃CN (0.75 mM) using *tert*-butyl acetate as an internal standard. [b] Binding constant determined by ¹H NMR titration. [c] Host point symmetry inferred from NMR spectroscopy. [d] The binding constant for *PP*-CRY (**G3'**) of $K_a = (2.40 \pm 0.10) \times 10^3$ M⁻¹ was identical within error.

Encouraged by the flexible nature of its S_4 -symmetric Fe^{II}₄L₄ framework and enclosed cavity, we next investigated the structural and stereochemical adaptability of **1** upon guest binding. Cage **1** was observed to bind both neutral and anionic guests (Table 1), with binding affinities quantified by ¹H NMR titrations, and binding stoichiometries gauged by NMR or ESI-MS, as detailed in Supporting Information Section 5.

Upon addition of tetraphenylborate **G1** or **G2**, the proton signals of **1** were observed to shift, in line with fast guest exchange on the NMR time scale (Figures S25 and S29). The signals of the cage furan and phenylene rings as well as the OMe groups at the apertures of **1** shifted most. In addition, when the central cavity of **1** (ca. 986 Å³) was occupied by **G3** (596 Å³) or **G4** (471 Å³), **1** was observed to bind **G1** (321 Å³) simultaneously, as shown in Figure 4. These observations led us to infer that **G1** and **G2** are bound peripherally at the edges of **1**.^[17c] The exact binding stoichiometries could not be gauged using ¹H NMR titrations (Figures S27 and S31), which fitted slightly, but not overwhelmingly better to a 1:2 model using BindFit.^[26] Chemical shift changes for **1** were plotted and fitted to a Hill function (Figures S28 and S32),^[27] with apparent association constants determined to be $(1.82 \pm 0.05) \times 10^2$ M⁻¹ and $(1.21 \pm 0.05) \times 10^2$ M⁻¹ for **G1** and **G2**, respectively. In both cases, the Hill coefficients were approximately 1, indicating non-cooperative binding of tetraphenylborates to **1**. Putative peripheral binding of tetraphenylborates during the titration process did not alter the S_4 symmetry of the framework of **1** (Figure 3b).

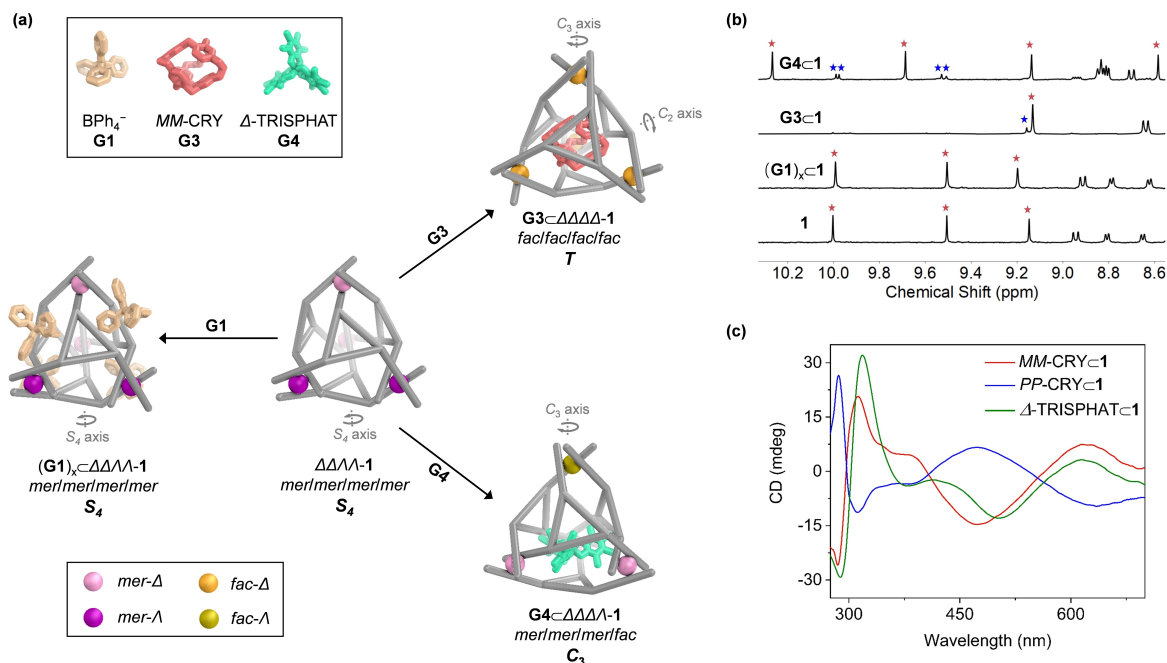


Figure 3. a) Schematic diagram showing the symmetry and stereochemical adaptation of **1** driven by guest binding. b) Partial ¹H NMR spectra of the imine region of **1** and its host–guest complexes (400 MHz, CD₃CN, 298 K), with imine peaks marked by stars. For **G3**⊂**1** and **G4**⊂**1**, red stars correspond to the major host–guest complex diastereomer (**G3**⊂ $\Delta\Delta\Delta\Delta-1$ or **G4**⊂ $\Delta\Delta\Delta\Lambda-1$), whereas blue stars correspond to the minor diastereomer with an enantiomorphous host configuration. c) CD spectra of host–guest complexes in acetonitrile at equal concentrations.

By contrast, enantiopure guest **G3**, *MM*-cryptophane (CRY),^[25,28] with a calculated volume of 596 Å³ was observed to bind centrally within the cavity of **1** in slow exchange on the NMR time scale, with a binding constant of $(2.33 \pm 0.10) \times 10^3 \text{ M}^{-1}$ (Figures 3a and S33). During titration experiments, proton signals corresponding to **G3**⊂**1** emerged as free **1** disappeared from the ¹H NMR spectrum. NMR integration revealed the formation of a 1:1 host–guest complex. All proton signals from the bound guest shifted significantly upfield as a result of shielding effects, consistent with central binding of **G3** (Figure S35). Interestingly, cage **1** was not observed to encapsulate C₆₀ (549 Å³), which we attribute to a poor fit between the bumpy inner surface of the host and the smooth curvature of the guest, precluding effective stacking interactions between them.

The ¹H NMR spectrum of **G3**⊂**1** was consistent with the formation of a *T*-symmetric species (Figures 3b and S35), with ligands in a threefold-symmetric environment and all metal centers adopting *facial* (*fac*) stereochemical configurations with the same handedness, as observed in high-symmetry face-capped tetrahedra.^[29] The presence of *fac* stereochemistry was also confirmed by the absence of characteristic NOE correlations between protons on the pyridyl and phenylene rings (Figure S38).

Two groups of proton peaks in a ratio of 4.8:1 were observed in the ¹H NMR spectrum, indicating that **G3**⊂**1** existed as a pair of diastereomers, *MM*-CRY⊂*AAAA*-**1** and *MM*-CRY⊂*AAAA*-**1**. The circular dichroism (CD) spectrum of **G3**⊂**1** displayed strong Cotton effects in the ranges 280–400 nm and 410–680 nm, assigned to π - π^* and metal-to-ligand charge transfer (MLCT) transitions, respectively (Figure 3c). The negative sign of the MLCT bands correlates with Δ handedness,^[30] suggesting that the major diastereomer of *MM*-CRY⊂**1** has four *fac-A* metal vertices. Cage **1** also bound the enantiomer *PP*-CRY to yield *PP*-CRY⊂**1** possessing four *fac-A* metal centers as the major diastereomer, with an identical-within-error binding affinity of $K_a = (2.40 \pm 0.10) \times 10^3 \text{ M}^{-1}$ (Figures S34 and S40).

Host-guest investigations also revealed that **1** was able to accommodate an equimolar amount of Δ -tris(tetrachloro-1,2-benzenediolato)phosphate (Δ -TRISPHAT, **G4**)^[31] with a binding affinity of $K_a = (1.17 \pm 0.15) \times 10^5 \text{ M}^{-1}$. When more than one equivalent of Δ -TRISPHAT was added during NMR titrations, no further changes were observed in ¹H and ³¹P NMR spectra (Figures S44 and S45), consistent with the formation of a 1:1 host–guest complex **G4**⊂**1**, as was also observed by ESI-MS (Figure S51). The ¹H NMR spectrum had two groups of signals, with each group containing four sets of signals (Figures 3b and S46), consistent with the presence of two C₃-symmetric diastereomers of **G4**⊂**1** in a 4.1:1 ratio. NOE correlations provided evidence for a 1:3 *fac:mer* configuration of metal centers for the major diastereomer (Figure S49), while the MLCT bands in the CD spectrum indicated an excess of Δ stereochemistry within **G4**⊂**1** (Figure 3c). We thus inferred that the major diastereomer of **G4**⊂**1** with C₃ symmetry contains one *fac-A* and three *mer-A* metal centers, as in the elegant “sorting hat” structure reported by Hooley and co-workers.^[32]

The conversion of S₄-symmetric **1** into *T*- and C₃-symmetric host–guest complexes did not occur at low temperatures, requiring to be heated at 343 K for 2 h to complete these transformations. The high temperatures required to overcome the energy barriers for this symmetry breaking and rearranging suggested a mechanism involving extensive disassembly and reassembly.^[33]

Having identified that **1** has two distinct binding sites that can bind different guests, we then explored allosteric effects by simultaneously treating **1** with two different guests (Figure 4). To consider cooperative effects, we determined the factor $\alpha = K'_a/K_a$ to quantify allosteric regulation, where K'_a and K_a are the binding constants of a guest bound by the host–guest complex and the empty host, respectively. A value of $\alpha > 1$ indicates positive cooperativity, whereas $\alpha < 1$ suggests negative cooperativity.^[2,26a]

Both *T*-symmetric **G3**⊂**1** and C₃-symmetric **G4**⊂**1** maintained their symmetries upon binding tetraphenylborate in fast exchange on the NMR time scale (Figure 4). Negative cooperativity ($\alpha = 0.59$ and 0.74) was observed in both cases (Figures S52–S57). When **1** bound BPh₄[−] peripherally, the central binding of both **G3** and **G4** was likewise inhibited. Negative cooperative effects ($\alpha = 0.60$ and 0.81) were observed on the binding of these two guests, which gave rise to *T*-symmetric **G3**·(**G1**)_x⊂**1** and C₃-symmetric **G4**·(**G1**)_x⊂**1**, respectively (Figures S58 and S59). This negative cooperativity was inferred to be a consequence of changes in aperture size and cavity volumes that took place in order to optimize binding, but which do not favor the binding of two guests at once. The binding of **G3** or **G4** within the cavity of **1** may also physically block **G1** from reaching inside the windows to bind. The presence of an electron-rich anionic or neutral guests within electron-deficient **1** may also weaken the binding of further electron-rich guests by electrostatic repulsion.

The higher binding affinity of **G4** over **G3** allowed for guest displacement, thus enabling the conversion of the *T*-symmetric cage framework into the C₃-symmetric one

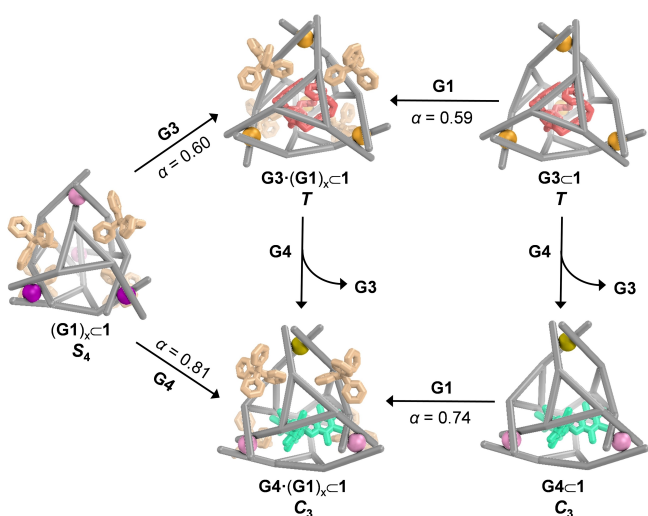


Figure 4. Schematic showing the allosteric effects and cooperative binding.

(Figures S60 and S61). The most strongly-binding guest in the system thus dictated the framework symmetry.

The ability of **1** to adopt three distinct diastereomeric conformations in order to optimize guest binding, including the singular S_4 framework, with two *mer-Δ* and two *mer-Λ* metal vertices, thus complements and builds usefully upon previous studies of cage stereochemistry. Its two allosterically active sites enabled the simultaneous binding of two distinct guests, peripherally and centrally. Future work may enable such allosteric effects to control reactions that are catalyzed within the cage cavity or at a peripheral site, potentially allowing up- or down-regulation of catalysis in biomimetic fashion.

Acknowledgements

This study was supported by the European Research Council (695009) and the UK Engineering and Physical Sciences Research Council (EPSRC, EP/T031603/1 and EP/P027067/1). W.X. thanks the Deutsche Forschungsgemeinschaft (DFG) for a postdoctoral fellowship. N.O. acknowledges the Chinese Scholarship Council (CSC) and Cambridge Trusts for MPhil funding. We thank the Yusuf Hamied Department of Chemistry NMR facility, University of Cambridge, for performing some NMR experiments, and Diamond Light Source (UK) for synchrotron beamtime on I19 (CY21497).

Conflict of Interest

The authors declare no conflict of interest.

Data Availability Statement

The data that support the findings of this study are available in the Supporting Information of this article.

Keywords: Allosteric Regulation • Host–Guest Chemistry • Metal–Organic Cages • Structural Adaptation • Symmetry

- [1] D. E. Koshland, Jr., *Angew. Chem. Int. Ed.* **1994**, *33*, 2375–2378; *Angew. Chem.* **1994**, *106*, 2468–2472.
- [2] a) C. A. Hunter, H. L. Anderson, *Angew. Chem. Int. Ed.* **2009**, *48*, 7488–7499; *Angew. Chem.* **2009**, *121*, 7624–7636; b) A. S. Mahadevi, G. N. Sastry, *Chem. Rev.* **2016**, *116*, 2775–2825.
- [3] a) C. Colombaro, G. Szalóki, M. Allain, L. Gómez, S. Goeb, M. Sallé, M. Costas, X. Ribas, *Chem. Eur. J.* **2017**, *23*, 3016–3022; b) R. Djemili, L. Kocher, S. Durot, A. Peuronen, K. Rissanen, V. Heitz, *Chem. Eur. J.* **2019**, *25*, 1481–1487; c) V. Martí-Centelles, R. L. Spicer, P. J. Lusby, *Chem. Sci.* **2020**, *11*, 3236–3240.
- [4] a) A. M. Lifshitz, M. S. Rosen, C. M. McGuirk, C. A. Mirkin, *J. Am. Chem. Soc.* **2015**, *137*, 7252–7261; b) P. W. J. M. Frederix, I. Patmanidis, S. J. Marrink, *Chem. Soc. Rev.* **2018**, *47*, 3470–3489; c) F. J. Rizzuto, L. K. S. von Krbek, J. R. Nitschke, *Nat. Chem. Rev.* **2019**, *3*, 204–222; d) A. E. Martín Díaz, J. E. Lewis, *Front. Chem.* **2021**, *9*, 706462.
- [5] For selected examples on molecular sensing and recognition, see: a) W. Xuan, M. Zhang, Y. Liu, Z. Chen, Y. Cui, *J. Am. Chem. Soc.* **2012**, *134*, 6904–6907; b) J. Dong, Y. Zhou, F. Zhang, Y. Cui, *Chem. Eur. J.* **2014**, *20*, 6455–6461; c) A. J. Plajer, E. G. Percástegui, M. Santella, F. J. Rizzuto, Q. Gan, B. W. Laursen, J. R. Nitschke, *Angew. Chem. Int. Ed.* **2019**, *58*, 4200–4204; *Angew. Chem.* **2019**, *131*, 4244–4248; d) T. R. Schulte, J. J. Holstein, G. H. Clever, *Angew. Chem. Int. Ed.* **2019**, *58*, 5562–5566; *Angew. Chem.* **2019**, *131*, 5618–5622; e) P. Howlader, E. Zangrando, P. S. Mukherjee, *J. Am. Chem. Soc.* **2020**, *142*, 9070–9078.
- [6] For selected examples and reviews on chemical separation, see: a) K. Wu, K. Li, Y.-J. Hou, M. Pan, L.-Y. Zhang, L. Chen, C.-Y. Su, *Nat. Commun.* **2016**, *7*, 10487; b) C. Fuertes-Espinosa, A. Gomez-Torres, R. Morales-Martinez, A. Rodriguez-Fortea, C. Garcia-Simon, F. Gandara, I. Imaz, J. Juanhuix, D. Maspoch, J. M. Poblet, L. Echegoyen, X. Ribas, *Angew. Chem. Int. Ed.* **2018**, *57*, 11294–11299; *Angew. Chem.* **2018**, *130*, 11464–11469; c) C. Fuertes-Espinosa, M. Pujals, X. Ribas, *Chem* **2020**, *6*, 3219–3262; d) D. Zhang, T. K. Ronson, Y.-Q. Zou, J. R. Nitschke, *Nat. Chem. Rev.* **2021**, *5*, 168–182; e) A. B. Sainaba, M. Venkateswarulu, P. Bhandari, K. S. A. Arachchige, J. K. Clegg, P. S. Mukherjee, *J. Am. Chem. Soc.* **2022**, *144*, 7504–7513.
- [7] For selected examples and reviews on stabilizing reactive species, see: a) P. Mal, B. Breiner, K. Rissanen, J. R. Nitschke, *Science* **2009**, *324*, 1697–1699; b) M. Yamashina, Y. Sei, M. Akita, M. Yoshizawa, *Nat. Commun.* **2014**, *5*, 4662; c) A. Galan, P. Ballester, *Chem. Soc. Rev.* **2016**, *45*, 1720–1737; d) S. Hasegawa, S. L. Meichsner, J. J. Holstein, A. Baksi, M. Kasanmascheff, G. H. Clever, *J. Am. Chem. Soc.* **2021**, *143*, 9718–9723.
- [8] For selected examples and reviews on cage catalysis, see: a) M. Yoshizawa, M. Tamura, M. Fujita, *Science* **2006**, *312*, 251–254; b) C. J. Brown, R. G. Bergman, K. N. Raymond, *J. Am. Chem. Soc.* **2009**, *131*, 17530–17531; c) C. García-Simón, R. Gramage-Doria, S. Raoufmoghaddam, T. Parella, M. Costas, X. Ribas, J. N. H. Reek, *J. Am. Chem. Soc.* **2015**, *137*, 2680–2687; d) D. M. Kaphan, M. D. Levin, R. G. Bergman, K. N. Raymond, F. D. Toste, *Science* **2015**, *350*, 1235–1238; e) W. Cullen, M. C. Misuraca, C. A. Hunter, N. H. Williams, M. D. Ward, *Nat. Chem.* **2016**, *8*, 231–236; f) W. Cullen, A. J. Metherell, A. B. Wragg, C. G. P. Taylor, N. H. Williams, M. D. Ward, *J. Am. Chem. Soc.* **2018**, *140*, 2821–2828; g) C. Tan, D. Chu, X. Tang, Y. Liu, W. Xuan, Y. Cui, *Chem. Eur. J.* **2019**, *25*, 662–672; h) J. Guo, Y.-Z. Fan, Y.-L. Lu, S.-P. Zheng, C.-Y. Su, *Angew. Chem. Int. Ed.* **2020**, *59*, 8661–8669; *Angew. Chem.* **2020**, *132*, 8739–8747; i) M. Morimoto, S. M. Bierschenk, K. T. Xia, R. G. Bergman, K. N. Raymond, F. D. Toste, *Nat. Catal.* **2020**, *3*, 969–984; j) G. Olivo, G. Capocasa, D. Del Giudice, O. Lanzalunga, S. Di Stefano, *Chem. Soc. Rev.* **2021**, *50*, 7681–7724; k) C. Ngai, H.-T. Wu, B. da Camara, C. G. Williams, L. J. Mueller, R. R. Julian, R. J. Hooley, *Angew. Chem. Int. Ed.* **2022**, *61*, e202117011; *Angew. Chem.* **2022**, *134*, e202117011.
- [9] a) W. Wang, Y.-X. Wang, H.-B. Yang, *Chem. Soc. Rev.* **2016**, *45*, 2656–2693; b) J. D. Crowley, L. S. Lisboa, Q. V. C. van Hilst in *Comprehensive Coordination Chemistry III* (Eds.: E. C. Constable, G. Parkin, L. Que, Jr.), Elsevier, Oxford, **2021**, pp. 174–205.
- [10] D. Zhang, T. K. Ronson, S. Güryel, J. D. Thoburn, D. J. Wales, J. R. Nitschke, *J. Am. Chem. Soc.* **2019**, *141*, 14534–14538.
- [11] H. Lee, J. Tessarolo, D. Langbehn, A. Baksi, R. Herges, G. H. Clever, *J. Am. Chem. Soc.* **2022**, *144*, 3099–3105.

- [12] V. Croué, S. Goeb, G. Szalóki, M. Allain, M. Sallé, *Angew. Chem. Int. Ed.* **2016**, *55*, 1746–1750; *Angew. Chem.* **2016**, *128*, 1778–1782.
- [13] L. S. Lisboa, J. A. Findlay, L. J. Wright, C. G. Hartinger, J. D. Crowley, *Angew. Chem. Int. Ed.* **2020**, *59*, 11101–11107; *Angew. Chem.* **2020**, *132*, 11194–11200.
- [14] a) R. W. Saalfrank, A. Stark, K. Peters, H. G. von Schnering, *Angew. Chem. Int. Ed. Engl.* **1988**, *27*, 851–853; *Angew. Chem.* **1988**, *100*, 878–880; b) D. L. Caulder, R. E. Powers, T. N. Parac, K. N. Raymond, *Angew. Chem. Int. Ed.* **1998**, *37*, 1840–1843; *Angew. Chem.* **1998**, *110*, 1940–1943; c) P. Mal, D. Schultz, K. Beyeh, K. Rissanen, J. R. Nitschke, *Angew. Chem. Int. Ed.* **2008**, *47*, 8297–8301; *Angew. Chem.* **2008**, *120*, 8421–8425; d) Y. Liu, X. Wu, C. He, Y. Jiao, C. Duan, *Chem. Commun.* **2009**, 7554–7556; e) L.-L. Yan, C.-H. Tan, G.-L. Zhang, L.-P. Zhou, J.-C. Bünzli, Q.-F. Sun, *J. Am. Chem. Soc.* **2015**, *137*, 8550–8555.
- [15] a) M. Fujita, D. Oguro, M. Miyazawa, H. Oka, K. Yamaguchi, K. Ogura, *Nature* **1995**, *378*, 469–471; b) P. J. Stang, B. Olenyuk, D. C. Muddiman, R. D. Smith, *Organometallics* **1997**, *16*, 3094–3096; c) O. Chepelin, J. Ujma, X. Wu, A. M. Z. Slawin, M. B. Pitak, S. J. Coles, J. Michel, A. C. Jones, P. E. Barran, P. J. Lusby, *J. Am. Chem. Soc.* **2012**, *134*, 19334–19337.
- [16] a) I. S. Tidmarsh, T. B. Faust, H. Adams, L. P. Harding, L. Russo, W. Clegg, M. D. Ward, *J. Am. Chem. Soc.* **2008**, *130*, 15167–15175; b) W. Meng, B. Breiner, K. Rissanen, J. D. Thoburn, J. K. Clegg, J. R. Nitschke, *Angew. Chem. Int. Ed.* **2011**, *50*, 3479–3483; *Angew. Chem.* **2011**, *123*, 3541–3545; c) X.-P. Zhou, J. Liu, S.-Z. Zhan, J.-R. Yang, D. Li, K.-M. Ng, R. W.-Y. Sun, C.-M. Che, *J. Am. Chem. Soc.* **2012**, *134*, 8042–8045; d) Y. Yang, J.-H. Jia, X.-L. Pei, H. Zheng, Z.-A. Nan, Q.-M. Wang, *Chem. Commun.* **2015**, *51*, 3804–3807.
- [17] a) B. Olenyuk, J. A. Whiteford, A. Fechtenkötter, P. J. Stang, *Nature* **1999**, *398*, 796–799; b) K. Ghosh, J. Hu, H. S. White, P. J. Stang, *J. Am. Chem. Soc.* **2009**, *131*, 6695–6697; c) F. J. Rizzuto, J. R. Nitschke, *Nat. Chem.* **2017**, *9*, 903–908.
- [18] a) M. Wang, C. Wang, X.-Q. Hao, X. Li, T. J. Vaughn, Y.-Y. Zhang, Y. Yu, Z.-Y. Li, M.-P. Song, H.-B. Yang, X. Li, *J. Am. Chem. Soc.* **2014**, *136*, 10499–10507; b) M. Han, Y. Luo, B. Damaschke, L. Gómez, X. Ribas, A. Jose, P. Peretzki, M. Seibt, G. H. Clever, *Angew. Chem. Int. Ed.* **2016**, *55*, 445–449; *Angew. Chem.* **2016**, *128*, 456–460; c) D. Fujita, Y. Ueda, S. Sato, H. Yokoyama, N. Mizuno, T. Kumasaka, M. Fujita, *Chem* **2016**, *1*, 91–101; d) D. Luo, X.-Z. Wang, C. Yang, X.-P. Zhou, D. Li, *J. Am. Chem. Soc.* **2018**, *140*, 118–121; e) H. Wang, K. Wang, Y. Xu, W. Wang, S. Chen, M. Hart, L. Wojtas, L.-P. Zhou, L. Gan, X. Yan, Y. Li, J. Lee, X.-S. Ke, X.-Q. Wang, C.-W. Zhang, S. Zhou, T. Zhai, H.-B. Yang, M. Wang, J. He, Q.-F. Sun, B. Xu, Y. Jiao, P. J. Stang, J. L. Sessler, X. Li, *J. Am. Chem. Soc.* **2021**, *143*, 5826–5835.
- [19] a) J. E. M. Lewis, J. D. Crowley, *ChemPlusChem* **2020**, *85*, 815–827; b) C. T. McTernan, J. A. Davies, J. R. Nitschke, *Chem. Rev.* **2022**, *122*, 10393–10437; c) J. E. M. Lewis, *Chem. Commun.* **2022**, *58*, 13873–13886.
- [20] Y. Tamura, H. Takezawa, M. Fujita, *J. Am. Chem. Soc.* **2020**, *142*, 5504–5508.
- [21] F. J. Rizzuto, P. Pröhm, A. J. Plajer, J. L. Greenfield, J. R. Nitschke, *J. Am. Chem. Soc.* **2019**, *141*, 1707–1715.
- [22] a) M. Hardy, M. Engeser, A. Lützen, *Beilstein J. Org. Chem.* **2020**, *16*, 2701–2708; b) Q. Shi, X. Zhou, W. Yuan, X. Su, A. Neniškis, X. Wei, L. Taujienis, G. Snarskis, J. S. Ward, K. Rissanen, J. de Mendoza, E. Orentas, *J. Am. Chem. Soc.* **2020**, *142*, 3658–3670.
- [23] C. A. Tolman, *Chem. Soc. Rev.* **1972**, *1*, 337–353.
- [24] A. J. McConnell, C. M. Aitchison, A. B. Grommet, J. R. Nitschke, *J. Am. Chem. Soc.* **2017**, *139*, 6294–6297.
- [25] J. B. Maglic, R. Lavendomme, *J. Appl. Crystallogr.* **2022**, *55*, 1033–1044.
- [26] a) P. Thordarson, *Chem. Soc. Rev.* **2011**, *40*, 1305–1323; b) H. Takezawa, T. Murase, G. Resnati, P. Metrangolo, M. Fujita, *J. Am. Chem. Soc.* **2014**, *136*, 1786–1788; c) D. Brynn Hibbert, P. Thordarson, *Chem. Commun.* **2016**, *52*, 12792–12805.
- [27] G. Ercolani, *J. Am. Chem. Soc.* **2003**, *125*, 16097–16103.
- [28] a) Van der Waals Volume of MM-cryptophane was calculated by MoloVol program, using reported crystal structures, see: T. Buffeteau, D. Pitrat, N. Daugey, N. Calin, M. Jean, N. Vanthuyne, L. Ducasse, F. Wien, T. Brotin, *Phys. Chem. Chem. Phys.* **2017**, *19*, 18303–18310; b) D. Zhang, A. Martinez, J.-P. Dutasta, *Chem. Rev.* **2017**, *117*, 4900–4942.
- [29] a) C. M. Hong, D. M. Kaphan, R. G. Bergman, K. N. Raymond, F. D. Toste, *J. Am. Chem. Soc.* **2017**, *139*, 8013–8021; b) D. Zhang, T. K. Ronson, J. L. Greenfield, T. Brotin, P. Berthault, E. Léonce, J.-L. Zhu, L. Xu, J. R. Nitschke, *J. Am. Chem. Soc.* **2019**, *141*, 8339–8345; c) S.-J. Hu, X.-Q. Guo, L.-P. Zhou, D.-N. Yan, P.-M. Cheng, L.-X. Cai, X.-Z. Li, Q.-F. Sun, *J. Am. Chem. Soc.* **2022**, *144*, 4244–4253.
- [30] a) S. E. Howson, L. E. N. Allan, N. P. Chmel, G. J. Clarkson, R. J. Deeth, A. D. Faulkner, D. H. Simpson, P. Scott, *Dalton Trans.* **2011**, *40*, 10416–10433; b) J. M. Dagna, G. Pescitelli, L. Tran, V. M. Lynch, E. V. Anslyn, L. Di Bari, *J. Am. Chem. Soc.* **2012**, *134*, 4398–4407.
- [31] J. Lacour, C. Ginglinger, C. Grivet, G. Bernardinelli, *Angew. Chem. Int. Ed.* **1997**, *36*, 608–610; *Angew. Chem.* **1997**, *109*, 660–662.
- [32] M. C. Young, L. R. Holloway, A. M. Johnson, R. J. Hooley, *Angew. Chem. Int. Ed.* **2014**, *53*, 9832–9836; *Angew. Chem.* **2014**, *126*, 9990–9994.
- [33] W. Meng, J. K. Clegg, J. D. Thoburn, J. R. Nitschke, *J. Am. Chem. Soc.* **2011**, *133*, 13652–13660.
- [34] Deposition Numbers 2235215 (for cage **3**) contains the supplementary crystallographic data for this paper. These data are provided free of charge by the joint Cambridge Crystallographic Data Centre and Fachinformationszentrum Karlsruhe Access Structures service.

Manuscript received: January 26, 2023
Accepted manuscript online: March 3, 2023
Version of record online: March 28, 2023